Sequential Estimation of Dynamic Deformation Parameters for SBAS-InSAR

Baohang Wang, Chaoying Zhao, Qin Zhang, Zhong Lu, Zhenhong Li, and Yuanyuan Liu

***Abstract*— The synthetic aperture radar (SAR) interferometry (InSAR) has been developed for more than 20 years for historical surface deformation reconstruction. In particular, the onboard Sentinel-1/A/B satellite, newly planned NASA-ISRO SAR (NISAR), and Germany Tandem-L will continue to provide unprecedented SAR data with an increased number of acquisitions. However, processing of real-time SAR data has been experiencing challenges regarding the InSAR deformation parameter estimation over a long time with the small baseline subsets (SBAS) InSAR technology. We use sequential adjustment for the estimation of the deformation parameters, which uses Bayesian estimation theory under the least square criteria to inverse long time-series deformation dynamically. Finally, both simulated and real Sentinel-1A SAR data verify the performance of the sequential estimation. It can be regarded as an effective data processing tool in the coming era of SAR big data.**

***Index Terms*— Bayesian estimation, dynamic deformation parameter estimation, InSAR time-series, least square (LS), sequential estimation.**

I. Introduction

THE synthetic aperture radar (SAR) interferometry (InSAR) provides unprecedented tools for wide-range deformation monitoring. However, the accuracy of the repeat-pass InSAR depends considerably on the coherence of the interferometric phases. To overcome the effect of decorrelation, the permanent scatterers (PS) [1] and small baseline subsets (SBAS) techniques [2] have been developed for retrieving the deformation history. For a more detailed comparison among different time-series InSAR methods, the readers can refer to [3].

Manuscript received June 25, 2019; revised August 23, 2019; accepted August 26, 2019. This work was supported in part by the National Key Research and Development Program of China under Grant 2018YFC1504805, in part by the Natural Science Foundation of China under Grant 41874005 and Grant 41731066, and in part by the Fundamental Research Funds for the Central Universities under Grant 300102269303 and Grant 300102269719. *(Corresponding author: Chaoying Zhao.)*

B. Wang is with the School of Geology Engineering and Geomatics, Chang'an University, Xi'an 710054, China (e-mail: baohangwang@163.com).

C. Zhao and Q. Zhang are with the School of Geology Engineering and Geomatics, Chang'an University, Xi'an 710054, China, and also with the National Administration of Surveying, Mapping and Geoinformation, Engineering Research Center of National Geographic Conditions Monitoring, Xi'an, 710054, China (e-mail: zhaochaoying@163.com; zhangqinle@263.net.cn).

Z. Lu is with the Roy M. Huffington Department of Earth Sciences, Southern Methodist University, Dallas, TX 75205 USA (e-mail: zhonglu@mail.smu.edu).

Z. Li is with the School of Geology Engineering and Geomatics, Chang'an University, Xi'an 710054, China, and also with the Civil Engineering Geomatics School of Engineering, Newcastle University, Newcastle Upon Tyne NE1 7RU, U.K. (e-mail: zhenhong.li@ncl.ac.uk).

Y. Liu is with the Faculty of Geomatics, East China University of Technology, Nanchang 200237, China (e-mail: yuanyuanolay@163.com).

Color versions of one or more of the figures in this letter are available online at http://ieeexplore.ieee.org.

Digital Object Identifier 10.1109/LGRS.2019.2938330

Moreover, with the advancement of the SAR satellites, the amount of the SAR data will continue to increase, and the revisit time will continue to decrease, which will promote the application of the SAR data in environment monitoring and disaster mitigation. The national-scale surface deformation monitoring in Italy and Germany was investigated [4], [5]. Accordingly, to improve the computational efficiency, the parallel computation strategy and the cloud-computing-based approach have been introduced to the SBAS InSAR processing [6], [7]. However, one problem that has arisen should be overcome in the big SAR data era, that is, the dynamical update of the deformation parameters without the loss of precision of the estimated parameters, which can also increase the computational efficiency of the SBAS InSAR processing. Recently, semiautomatic identification of the active clusters pixels method [8] and multi-baseline SAR interferograms-based sequential filter method [9] were proposed for the PS selection and noise reduction of phase.. Moreover, the Kalman filter method was proposed for the deformation estimation [10]. However, the inaccuracy of the prediction model leads to the deviation of the results.

For the time-series deformation inversion of the SBAS-InSAR technology, on one hand, all SAR data are processed repeatedly once each new SAR data are presented, which undoubtedly increases the computation burden due to the inverse operation of the large matrix, while most of the earlier deformation parameters are unchangeable for each SBAS InSAR processing. On the other hand, if we only inverse the deformation parameters with the fusion of newly observed SAR image and partial previously processed SAR images, the previous deformation results cannot be precisely linked through cofactor matrix, which results in the inconsistency of the deformation estimations.

Therefore, we will introduce a sequential adjustment to the SBAS InSAR processing to estimate the deformation parameters dynamically [11], [12], which can keep consistent accuracy with the traditional SBAS method but with high computation efficiency. To this end, the least square (LS) Bayesian estimation theory [12] is used. Finally, the performance of the new method is verified with both simulated and real Sentinel-1 SAR data.

II. Sequential Estimation

First, we use all SAR acquisitions to calculate the deformation time-series by the SBAS InSAR technique with single SBAS subset interferograms. The cofactor matrixes of the time-series deformation of each pixel are used to assess its accuracy. In the second step, once we acquire new SAR data, the former estimated deformation parameters and their

cofactor matrixes rather than original unwrapped interferograms are involved in sequential estimation to update the deformation parameters as quickly as possible.

A. Deformation Rate and Digital Elevation Model Error Estimation

After correcting the atmospheric artifacts, and orbital errors, we first estimate the deformation rate and digital elevation model (DEM) error from the unwrapped interferograms using the following function model:

$$\underbrace{\begin{bmatrix} \frac{4\pi}{\lambda \sin\theta}\frac{B_1^{\perp}}{R_1} & \frac{4\pi}{\lambda}T_1 \\ \vdots & \vdots \\ \frac{4\pi}{\lambda \sin\theta}\frac{B_M^{\perp}}{R_M} & \frac{4\pi}{\lambda}T_M \end{bmatrix}}_{\mathbf{A}_1} \underbrace{\begin{bmatrix} \Delta H \\ V \end{bmatrix}}_{X} = \underbrace{\begin{bmatrix} unw_1 \\ unw_2 \\ \vdots \\ unw_M \end{bmatrix}}_{L_1} \tag{1}$$

where V, ΔH, and unw denote the deformation rate, DEM error, and unwrapped interferometric phases, respectively. λ, R, and θ denote the radar wavelength, sensor-to-target distance, and incidence angle, respectively. $B_i^{\perp}$ and T_i ($i = 1, \ldots, M$) are the perpendicular baselines and temporal baselines between the master image and the ith image, respectively. M is the number of interferograms constructed by the SBAS InSAR processing. We can rewrite (1) in the matrix form as follows:

$$\boldsymbol{V}_1 = \mathbf{A}_1 \boldsymbol{X} - \boldsymbol{L}_1, \mathbf{P}_1 \tag{2}$$

where V_1 is the measurement noise, and $\mathbf{P}_1$ is the weight matrix. Then, the parameter $\boldsymbol{X}$, that is, the deformation rate and the DEM error, can be readily estimated with LS

$$\begin{aligned} \boldsymbol{X}^{(1)} &= \left(\mathbf{A}_1^T \mathbf{P}_1 \mathbf{A}_1\right)^{-1} \mathbf{A}_1^T \mathbf{P}_1 \boldsymbol{L}_1 \\ \boldsymbol{Q}_{X^{(1)}} &= \left(\mathbf{A}_1^T \mathbf{P}_1 \mathbf{A}_1\right)^{-1} \end{aligned} \tag{3}$$

where $\boldsymbol{X}^{(1)}$ indicates the first estimation of parameter $\boldsymbol{X}$, and $\boldsymbol{Q}_{X^{(1)}}$ is its cofactor matrix. The superscript T stands for the transpose of a matrix.

In the conventional SBAS InSAR processing, when we acquire new SAR data, the design matrix $\mathbf{A}_1$ is reconstructed by configuring all interferograms to estimate the parameters again. On the contrary, we use the sequential estimation to update the deformation parameters dynamically. We can write its observational equation as follows:

$$\boldsymbol{V}_2 = \mathbf{A}_2 \boldsymbol{X}^{(2)} - \boldsymbol{L}_2, \mathbf{P}_2 \tag{4}$$

where $\boldsymbol{X}^{(2)}$ indicates the second estimation of parameter $\boldsymbol{X}$, and $\boldsymbol{L}_2$, $\mathbf{A}_2$, $\boldsymbol{V}_2$, and $\mathbf{P}_2$ are the new observations (unwrapped interferograms related to the new SAR acquisition), design matrix, measurement error, and weight matrix, respectively.

We take $\boldsymbol{X}^{(1)}$ and $\boldsymbol{Q}_{X^{(1)}}$ as a prior information of the parameter $\boldsymbol{X}^{(2)}$. Hence, $\boldsymbol{V}_2$ and $\boldsymbol{X}^{(2)}$ obey the Gaussian distribution and independent each other as follows:

$$\begin{aligned} &\boldsymbol{V}_2 \sim N\left(0, \sigma_0^2 \mathbf{P}_2^{-1}\right) \\ &\boldsymbol{X}^{(2)} \sim N\left(\boldsymbol{X}_1, \sigma_0^2 \boldsymbol{Q}_{X^{(1)}}\right) \\ &Cov\left(\boldsymbol{V}_2, \boldsymbol{X}^{(2)}\right) = 0 \end{aligned} \tag{5}$$

where σ_0^2 is the unit weight variance.

According to the principle of classical LS Bayesian estimation [12], it holds

$$\boldsymbol{V}_2^T \mathbf{P}_2 \boldsymbol{V}_2 + (\boldsymbol{X}^{(2)} - \boldsymbol{X}^{(1)})^T \boldsymbol{Q}_{X^{(1)}}^{-1} (\boldsymbol{X}^{(2)} - \boldsymbol{X}^{(1)}) = \min . \tag{6}$$

The parameter $\boldsymbol{X}^{(2)}$ and its cofactor matrix $\boldsymbol{Q}_{X^2}$ are updated as follows [12]:

$$\begin{aligned} \boldsymbol{X}^{(2)} &= \left(\boldsymbol{Q}_{X^{(1)}}^{-1} + \mathbf{A}_2^T \mathbf{P}_2 \mathbf{A}_2\right)^{-1} \left(\boldsymbol{Q}_{X^{(1)}}^{-1} \boldsymbol{X}^{(1)} + \mathbf{A}_2^T \mathbf{P}_2 \boldsymbol{L}_2\right) \\ \boldsymbol{Q}_{X^{(2)}} &= \left(\boldsymbol{Q}_{X^{(1)}}^{-1} + \mathbf{A}_2^T \mathbf{P}_2 \mathbf{A}_2\right)^{-1}. \end{aligned} \tag{7}$$

We run the above-mentioned procedure iteratively to obtain the new parameters by considering the latest SAR acquisition.

B. Deformation Time-Series Estimation

After the DEM error is further corrected for the unwrapped interferograms, we estimate the time-series deformation phases using the following function model:

$$\underbrace{\begin{bmatrix} -1 & 1 & 0 & \ldots & 0 & 0 & 0 \\ -1 & 0 & 1 & \cdots & 0 & 0 & 0 \\ \vdots & \vdots & \vdots & \vdots & \vdots & \vdots & \vdots \\ 0 & 0 & 0 & \cdots & 0 & -1 & 1 \end{bmatrix}}_{\mathbf{A}_1} \underbrace{\begin{bmatrix} \varphi_1 \\ \varphi_2 \\ \vdots \\ \varphi_N \end{bmatrix}}_{X} = \underbrace{\begin{bmatrix} unw_1 \\ unw_2 \\ \vdots \\ unw_M \end{bmatrix}}_{L_1} \tag{8}$$

where $\varphi_i (i = 1, \ldots, N)$ denotes the deformation phase in the line-of-sight (LOS) direction at the different SAR acquisition date and $N+1$ is the number of SAR acquisitions. Note that the deformation at the first SAR acquisition date is zero, that is, $\varphi_0 = 0$. To estimate the deformation time-series, the archived SAR data modeled as (8) are rewritten in the same matrix form as (2) with different parameters $\boldsymbol{X}$ and design matrix $\mathbf{A}_1$. Then, we can calculate the first estimation $\boldsymbol{X}^{(1)}$ of the parameter $\boldsymbol{X}$ and its cofactor matrix $\boldsymbol{Q}_{X^{(1)}}$ as shown in (3).

When we acquire new SAR image, unlike the conventional SBAS InSAR constructs (8) and estimate deformation time-series again, we use the sequential estimation to update the deformation time-series dynamically by only considering the unwrapped interferograms related to the new SAR image. New measurement data are $\boldsymbol{L}_2$ (unwrapped interferograms related to the $(N+2)th$ new SAR acquisition) with weight matrix $\mathbf{P}_2$, design matrixes $\mathbf{A}_2$ and $\boldsymbol{B}$, and parameters $\boldsymbol{X}$ and $\boldsymbol{Y}$. We can write its observational equation as follows:

$$\boldsymbol{V}_2 = \begin{bmatrix} \mathbf{A}_2 & \boldsymbol{B} \end{bmatrix} \begin{bmatrix} \boldsymbol{X}^{(2)} \\ \boldsymbol{Y} \end{bmatrix} - \boldsymbol{L}_2, \quad \mathbf{P}_2 . \tag{9}$$

Because $\boldsymbol{Y}$ has no prior information, the parameters $\boldsymbol{X}^{(2)}$ and $\boldsymbol{Y}$ are estimated based on LS Bayesian estimation theory [12] as follows [11]:

$$\begin{aligned} \begin{bmatrix} \boldsymbol{X}^{(2)} \\ \boldsymbol{Y} \end{bmatrix} &= \begin{bmatrix} \boldsymbol{Q}_{X^{(1)}}^{-1} + \mathbf{A}_2^{\mathbf{T}} \mathbf{P}_2 \mathbf{A}_2 & \mathbf{A}_2^{\mathbf{T}} \mathbf{P}_2 \mathbf{A}_2 \\ \mathbf{B}^{\mathbf{T}} \mathbf{P}_2 \mathbf{A}_2 & \mathbf{B}^{\mathbf{T}} \mathbf{P}_2 \mathbf{B} \end{bmatrix}^{-1} \\ &\quad \times \begin{bmatrix} \boldsymbol{Q}_{X^{(1)}}^{-1} \boldsymbol{X}^{(1)} + \mathbf{A}_2^{\mathbf{T}} \mathbf{P}_2 \boldsymbol{L}_2 \\ \mathbf{B}^{\mathbf{T}} \mathbf{P}_2 \boldsymbol{L}_2 \end{bmatrix} \\ \boldsymbol{Q}_{[X^{(2)};Y]} &= \begin{bmatrix} \boldsymbol{Q}_{X^{(1)}}^{-1} + \mathbf{A}_2^{\mathbf{T}} \mathbf{P}_2 \mathbf{A}_2 & \mathbf{A}_2^{\mathbf{T}} \mathbf{P}_2 \mathbf{A}_2 \\ \mathbf{B}^{\mathbf{T}} \mathbf{P}_2 \mathbf{A}_2 & \mathbf{B}^{\mathbf{T}} \mathbf{P}_2 \mathbf{B} \end{bmatrix}^{-1} \end{aligned} \tag{10}$$

where $\boldsymbol{Q}_{[\hat{X}^{(2)};Y]}$ denotes the cofactor matrix of the parameter $\left[\hat{X}^{(2)}\ Y\right]^T$. In practice, to increase the computational efficiency in (7) and (10), the inverse of two matrices $(\boldsymbol{Q}^{-1}_{\hat{X}^{(1)}} + \mathbf{A}_2^T\mathbf{P}_2\mathbf{A}_2)$ and $\begin{bmatrix} \boldsymbol{Q}^{-1}_{\hat{X}^{(1)}} + \mathbf{A}_2^T\mathbf{P}_2\mathbf{A}_2 & \mathbf{A}_2^T\mathbf{P}_2\mathbf{A}_2 \\ \mathbf{B}^T\mathbf{P}_2\mathbf{A}_2 & \mathbf{B}^T\mathbf{P}_2\mathbf{B} \end{bmatrix}$ are simplified using the matrix inversion theory [11] as follows:

$$(\mathbf{P}_1 \pm \mathbf{A}^T\mathbf{P}_2\mathbf{A})^{-1} = \mathbf{P}_1^{-1} \mp \mathbf{P}_1^{-1}\mathbf{A}^T\left(\mathbf{P}_2^{-1} \pm \mathbf{A}^T\mathbf{P}_1^{-1}\mathbf{A}\right)^{-1}\mathbf{A}^T\mathbf{P}_1^{-1}. \tag{11}$$

Thus, we can rewrite (7) as follows:

$$\begin{aligned} \hat{X}^{(2)} &= \hat{X}^{(1)} + \mathbf{J}_x\bar{L}_2 \\ \boldsymbol{Q}_{\hat{X}^{(2)}} &= \boldsymbol{Q}_{\hat{X}^{(1)}} - \mathbf{J}_x\mathbf{A}_2\boldsymbol{Q}_{\hat{X}^{(1)}} \\ \bar{L}_2 &= L_2 - \mathbf{A}_2\hat{X}^{(1)} \end{aligned} \tag{12}$$

where $\hat{X}^{(2)}$ and $\boldsymbol{Q}_{\hat{X}^{(2)}}$ are the updated parameter and its cofactor matrix, respectively. $\mathbf{J}_x$ is the gain matrix, in which $\boldsymbol{Q}_J$ is the updated cofactor matrix with the newly presented image as following:

$$\begin{aligned} \mathbf{J}_x &= \boldsymbol{Q}_{\hat{X}^{(1)}}\mathbf{A}_2^T\boldsymbol{Q}_J^{-1} \\ \boldsymbol{Q}_J &= \mathbf{P}_2^{-1} + \mathbf{A}_2\boldsymbol{Q}_{\hat{X}^{(1)}}\mathbf{A}_2^T. \end{aligned} \tag{13}$$

Then, we can rewrite (10) as follows:

$$\begin{aligned} \begin{bmatrix} \hat{X}^{(2)} \\ Y \end{bmatrix} &= \begin{bmatrix} \hat{X}^{(1)} + \mathbf{J}_x(\bar{L}_2 - \mathbf{B}Y) \\ (\mathbf{B}^T\boldsymbol{Q}_J^{-1}\mathbf{B})^{-1}\mathbf{B}^T\boldsymbol{Q}_J^{-1}(L_2 - \mathbf{A}_2\hat{X}_1) \end{bmatrix} \\ \boldsymbol{Q}_{[\hat{X}^{(2)};Y]} &= \begin{bmatrix} \boldsymbol{Q}_{\hat{X}^{(2)}} & \boldsymbol{Q}_{\hat{X}^{(2)},Y} \\ -\boldsymbol{Q}_{\hat{X}^{(2)},Y} & \boldsymbol{Q}_Y \end{bmatrix} \\ \boldsymbol{Q}_{\hat{X}^{(2)}} &= \boldsymbol{Q}_{\hat{X}^{(1)}} - \mathbf{J}_x\mathbf{A}_2\boldsymbol{Q}_{\hat{X}^{(1)}} + \mathbf{J}_x\mathbf{B}\boldsymbol{Q}_Y\mathbf{B}^T\mathbf{J}_x^T \\ \boldsymbol{Q}_{\hat{X}^{(2)},Y} &= -\mathbf{J}_x\mathbf{B}\boldsymbol{Q}_{Y,Y} \\ \boldsymbol{Q}_Y &= (\mathbf{B}^T\boldsymbol{Q}_J\mathbf{B})^{-1} \end{aligned} \tag{14}$$

where $[\hat{X}^{(2)}; Y]$ $[\hat{X}^{(2)}Y]$ is the estimated deformation time-series, in which Y is the cumulative deformation for the new SAR acquisition, and $\boldsymbol{Q}_{[\hat{X}^{(2)};Y]}$ is their cofactor matrix. Hence, when the new SAR image is presented, (12) gives the final solution of the deformation rate and the DEM error by the sequential estimation, and (14) provides the deformation time-series estimation. Accordingly, we can update the deformation parameters as quickly as possible with these two equations.

The standard deviation (STD) of the estimated parameters can be estimated by the following equation:

$$\sigma_{[\hat{X}^{(2)};Y]} = \hat{\sigma}_0\sqrt{\boldsymbol{Q}_{[\hat{X}^{(2)};Y]}} \tag{15}$$

where the standard error unit weight $\hat{\sigma}_0$ can be estimated as

$$\hat{\sigma}_0 = \sqrt{\frac{V_2^T\mathbf{P}_2V_2 + (\hat{X}^{(2)} - \hat{X}^{(1)})^T\boldsymbol{Q}^{-1}_{\hat{X}^{(1)}}(\hat{X}^{(2)} - \hat{X}^{(1)})}{M_1 + M_2 - N}} \tag{16}$$

where M_1 and M_2 are the number of original interferograms and newly generated interferograms, respectively, and N is the number of the estimated parameters.

As the noise of the unwrapped phase obeys the Gaussian distribution, theoretical accuracy bound of the worst case in the sequential estimation can be given with twice or three times of the STD under different confidence intervals as

$$\begin{aligned} P(-2\sigma < \Delta < +2\sigma) &= 95.5\% \\ P(-3\sigma < \Delta < +3\sigma) &= 99.7\%. \end{aligned} \tag{17}$$

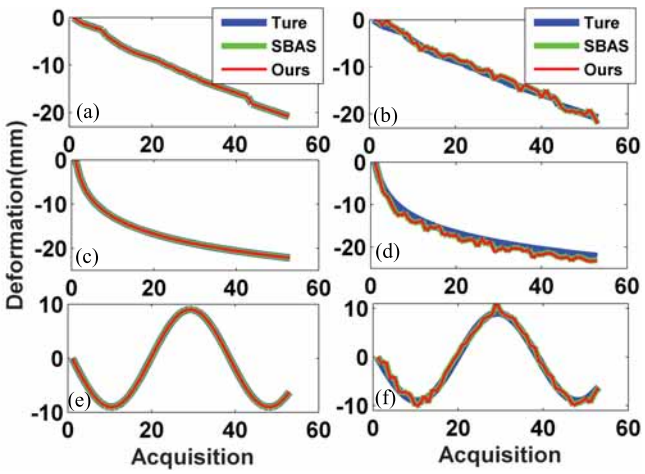

Fig. 1. Time-series deformation derived by the conventional SBAS (SBAS) and sequential estimation (ours) with three different deformation models. The left column is noise-free, while the right one includes noise. The blue, green, and red lines represent the true deformation, the deformation derived from the conventional SBAS, and the sequential estimation, respectively. (a) and (b) Linear model. (c) and (d) Exponential model. (e) and (f) Periodic model.

III. Experimental Test

A. Simulated Data

First, to demonstrate the sequential estimation, three deformation models including linear model, exponential model, and periodic model for one generic pixel are simulated. In total, 53 single look complex (SLC) images are considered, and 307 interferograms are constructed by setting the thresholds for the spatial and temporal baselines. We assume the first 30 SLCs are archived data, and the sequential estimation is carried out from the 31st SLC (May 28, 2017) to the 53rd SLC (April 29, 2019) to estimate the deformation parameters sequentially. Fig. 1 shows the three simulated deformation models with and without noise, and the estimation of the time-series deformation with the conventional SBAS and our methods.

To evaluate the accuracy of the results, the STD of the estimated parameters for both SBAS and sequential estimation are 0.1, 0.7, and 1.5 mm for three deformation models with noise levels $N \sim (0, 0.5)$, $N \sim (0, 2)$, and $N \sim (0, 4)$, respectively, by 1000 random simulations. The results show that the accuracy of the estimated parameters with our method is the same as the SBAS method.

B. Real Data

We use 53 Sentinel-1A SAR data covering Xi'an, China, to demonstrate the proposed algorithm. For a more detailed description of the selection of coherent points, initial DEM error estimation, and phase unwrapping in this InSAR preprocessing, the readers can refer to [13]. The deformation rate and the DEM error estimated by the sequential method are

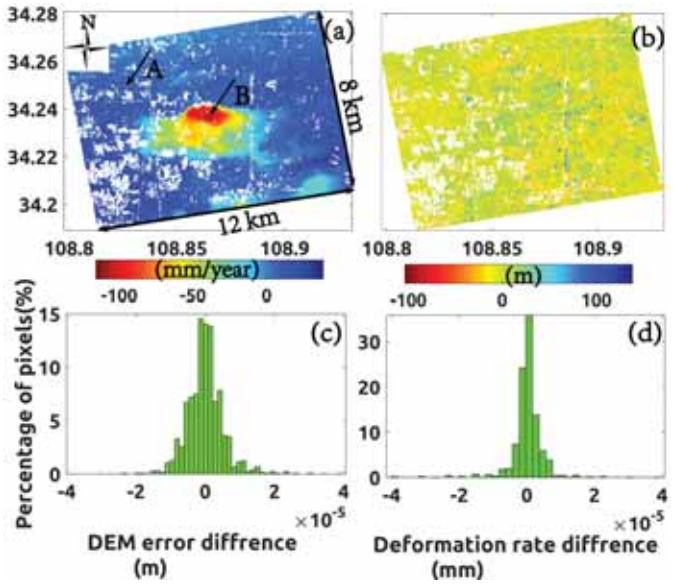

Fig. 2. Comparison of the deformation rate and DEM error derived by the sequential estimation and conventional SBAS. (a) and (b) Deformation rate and DEM error by the sequential estimation, respectively. (c) and (d) Difference histograms of the deformation rate and DEM error between the sequential estimation and the conventional SBAS, respectively.

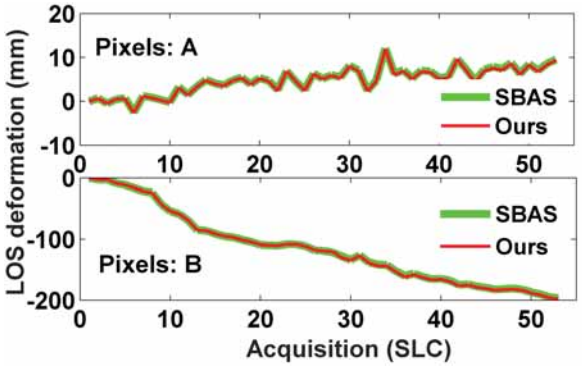

Fig. 3. Comparison of time-series deformation between the conventional SBAS and ours for pixels A and B shown in Fig. 3. Green line: deformation obtained from the conventional SBAS. Red line: result of our method.

shown in Fig. 2(a) and (b). The comparisons between the sequential estimation and the conventional SBAS are shown in Fig. 2(c) and (d), and it is shown that the result derived from the sequential estimation is entirely consistent with the conventional SBAS.

For the time series deformation, the pixel A is located in the slow deformation region in Fig. 2(a), while pixel B is located in the significant deformation region in Fig. 2(a), are analyzed (Fig. 3). It reveals that time-series deformation from the two methods is consistent as well.

Moreover, the cumulative time-series deformation from May 28, 2017 to April 29, 2019 (30th to 53rd SLCs) by the sequential estimation is shown in Fig. 4.

Qualitatively, Fig. 5 shows the histograms of the difference between the sequential estimation and the conventional SBAS from the whole scene, which verifies that the deformation time-series of the two methods is consistent and the difference between the two methods is negligible.

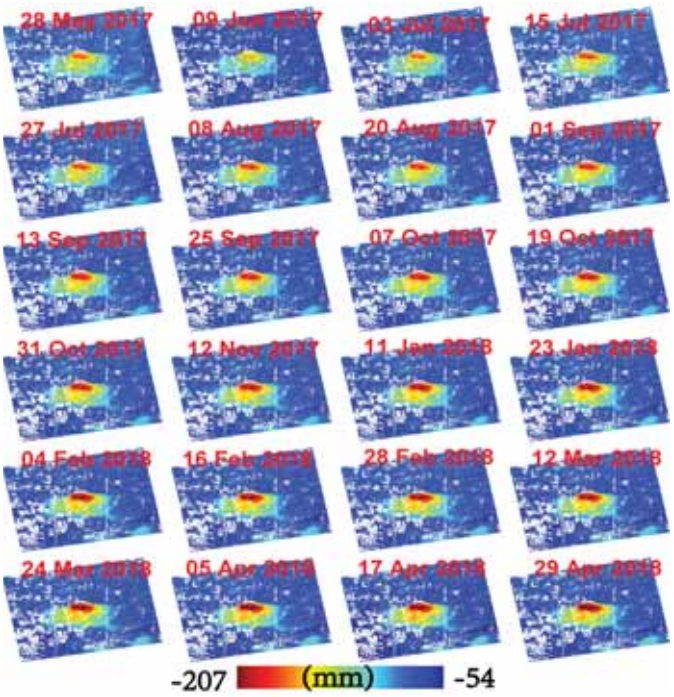

Fig. 4. Cumulative time-series deformation maps by the sequential estimation from May 28, 2017 to April 29, 2019 (the 30th SLC to the 53rd SLC acquisition).

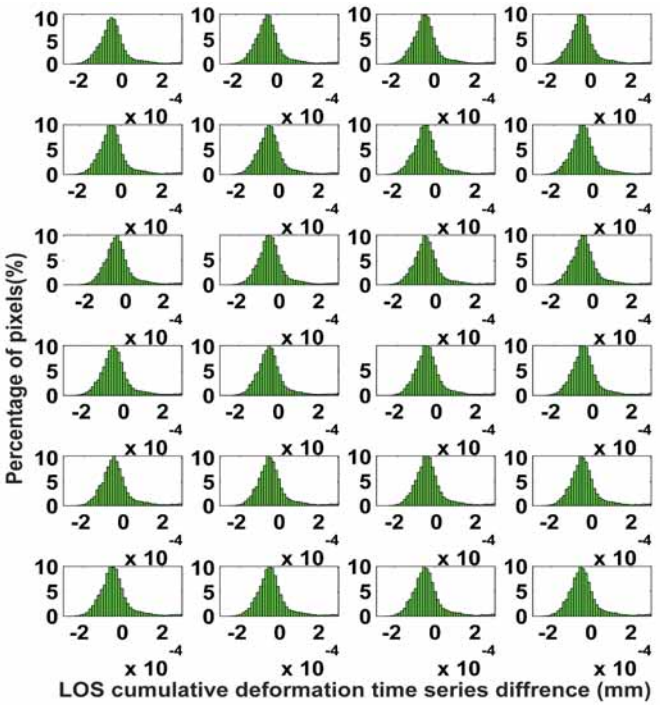

Fig. 5. Histograms of the difference of time-series deformation between the sequential estimation and the conventional SBAS from May 28, 2017 to April 29, 2019.

IV. Discussion

In theory, the sequential estimation is consistent with the conventional SBAS-InSAR method under the singular value decomposition (SVD) or LS criteria. The simulated different deformation models, with different noise levels, and the real

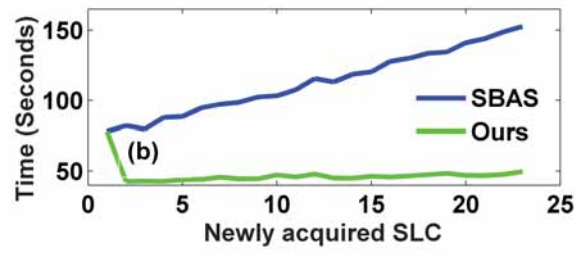

Fig. 6. Comparison of execution time by the conventional SBAS and the sequential estimation from May 28, 2017 to April 29, 2019 (corresponding to the 31st SLC to 53rd SLC acquisitions).

data verify that the sequential estimation can obtain the same optimal solution as the SBAS-InSAR processing for the whole unwrapped interferograms.

The advantage of the sequential estimation is that it can improve the computational efficiency significantly, especially for the massive SAR data processing, as it does not store all historical observations to estimate the deformation for the newly presented SAR image. Fig. 6 shows the execution time for the calculation of 50 000 pixels by the conventional SBAS and the sequential estimation methods. It shows that both the SBAS and sequential estimation methods spend the same time for the initialization of the deformation estimation with 30 SLC images. Afterward, the sequential estimation spends a very short time and keeps constant for the update of time-series deformation, while the SBAS method spends much more time than the sequential estimation and increases the execution time linearly with the increase of SAR data. The test was done based on MATLAB R2015b software and an Intel Xeon CPU E5-2640 v4 at the 2.40-GHz computer.

Besides, as for the application of the sequential estimation, we should take some attention as follows. First, to avoid the phase unwrapping errors caused by deformation gradient and decorrelation, the spatiotemporal baseline thresholds should be set with some *a priori* knowledge for the newly presented image and archived images to form new interferograms. Second, the systematic errors arising from the atmospheric effect and inaccurate baseline estimation should be corrected in advance. Third, the gross error caused by the unwrapping error should also be detected and mitigated. To this end, the weighted iterative LS (IRLS) method [14] and the adaptive factor α [15] can be considered for the weight matrix determination of P1 and P2.

V. Conclusion

We introduce the sequential estimation to the SBAS InSAR procedure to update the deformation parameters as quickly as possible. The sequential estimation is an effective tool for the InSAR dynamic deformation parameter estimation as it does not store massive unwrapped interferograms and solve the inversion of a large matrix. Both simulated and real SAR data demonstrate that this proposed method can get the deformation results with the same accuracy as the conventional SBAS-InSAR method. Therefore, this method can be expected to be used in the era of big SAR data.

Acknowledgment

Sentinel-1A data are copyrighted to the European Space Agency.

References

[1] A. Ferretti, C. Prati, and F. Rocca, "Permanent scatterers in SAR interferometry," *IEEE Trans. Geosci. Remote Sens.*, vol. 39, no. 1, pp. 8–20, Jan. 2001.

[2] P. Berardino, G. Fornaro, R. Lanari, and E. Sansosti, "A new algorithm for surface deformation monitoring based on small baseline differential SAR interferograms," *IEEE Trans. Geosci. Remote Sens.*, vol. 40, no. 11, pp. 2375–2383, Nov. 2002.

[3] B. Osmanoğlu, F. Sunar, S. Wdowinski, and E. Cabral-Cano, "Time series analysis of InSAR data: Methods and trends," *J. Photogramm. Remote Sens.*, vol. 115, pp. 90–102, May 2016.

[4] M. Costantini *et al.*, "Analysis of surface deformations over the whole Italian territory by interferometric processing of ERS, Envisat and COSMO-SkyMed radar data," *Remote Sens. Environ.*, vol. 202, pp. 250–275, Dec. 2017.

[5] A. C. Kalia, M. Frei, and T. Lege, "A copernicus downstream-service for the nationwide monitoring of surface displacements in Germany," *Remote Sens. Environ.*, vol. 202, pp. 234–249, Dec. 2017.

[6] I. Zinno, F. Casu, C. De Luca, S. Elefante, R. Lanari, and M. Manunta, "A cloud computing solution for the efficient implementation of the P-SBAS dinsar approach," *IEEE J. Sel. Topics Appl. Earth Observ. Remote Sens.*, vol. 10, no. 3, pp. 802–817, Mar. 2017.

[7] C. De Luca, I. Zinno, M. Manunta, R. Lanari, and F. Casu, "Large areas surface deformation analysis through a cloud computing P-SBAS approach for massive processing of DInSAR time series," *Remote Sens. Environ.*, vol. 202, pp. 3–17, Dec. 2017.

[8] R. Tomás *et al.*, "Semi-automatic identification and pre-screening of geological–geotechnical deformational processes using persistent scatterer interferometry datasets," *Remote Sens.*, vol. 11, no. 14, p. 1675, 2019.

[9] H. Ansari, F. De Zan, and R. Bamler, "Sequential estimator: Toward efficient InSAR time series analysis," *IEEE Trans. Geosci. Remote Sens.*, vol. 55, no. 10, pp. 5637–5652, Oct. 2017.

[10] J. Hu, X. L. Ding, Z. W. Li, J. J. Zhu, Q. Sun, and L. Zhang, "Kalman-filter-based approach for multisensor, multitrack, and multitemporal InSAR," *IEEE Trans. Geosci. Remote Sens.*, vol. 51, no. 7, pp. 4226–4239, Jul. 2013.

[11] [11] Huang. W. B, "Modern adjustment theory and its application," *PLA Press, Beijing*, China. 1992. (in Chinese).

[12] Y. Yuan Xi, "Robust Bayesian estimation," *J. Geodesy*, vol. 65, no. 3, pp. 145–150, 1991.

[13] A. Hooper, "A multi-temporal InSAR method incorporating both persistent scatterer and small baseline approaches," *Geophys. Res. Lett.*, vol. 35, no. 16, pp. 96–106, 2008.

[14] V. Akbari and M. Motagh, "Improved ground subsidence monitoring using small baseline SAR interferograms and a weighted least squares inversion algorithm," *IEEE Geosci. Remote Sens. Lett.*, vol. 9, no. 3, pp. 437–441, May 2012.

[15] Y. Yang, H. He, and G. Xu, "Adaptively robust filtering for kinematic geodetic positioning," *J. Geodesy*, vol. 75, pp. 109–116, May 2001.